JACS
JOURNAL OF THE AMERICAN CHEMICAL SOCIETY

Article

pubs.acs.org/JACS

Mechanical Stability of the Antibody Domain C_H3 Homodimer in Different Oxidation States

Morten Bertz,*[,†,∥] Johannes Buchner,[‡,§] and Matthias Rief[†,§]

[†]Physik Department E22, Technische Universität München, James-Franck-Straße 1, 85748 Garching, Germany
[‡]Chemie Department, Technische Universität München, Lichtenbergstraße 4, 85748 Garching, Germany
[§]Munich Center for Integrated Protein Science (CIPSM), 81377 München, Germany

Supporting Information

ABSTRACT: The C_H3 homodimer at the C-terminal end of the antibody heavy chain is the key noncovalent interaction stabilizing antibody proteins. Here, we use single-molecule force spectroscopy to investigate the dissociation mechanics of C_H3 as a proxy for antibody mechanical stability. We find the C_H3 homodimer to be a highly stable complex, and its dissociation force of >150 pN at a loading rate of ≈5500 pN/s exceeds the stability of most protein−protein interactions studied to date. Separated C_H3 monomers, on the other hand, are mechanically labile and only short-lived. Each C_H3 monomer contains a conserved buried disulfide bridge, and we find that the successive reduction of one or both disulfide bridges in the dimer results in a stepwise decrease of the dissociation force. This suggests a structural role of the disulfide bridges helping to mold the high-affinity domain−domain interface, even though they are neither required for nor directly involved in dimerization. Taken together, our results set a limit on how much force a single antibody can bear and reveal the C_H3 homodimer as a mechanical fastener that prevents antibody dissociation.

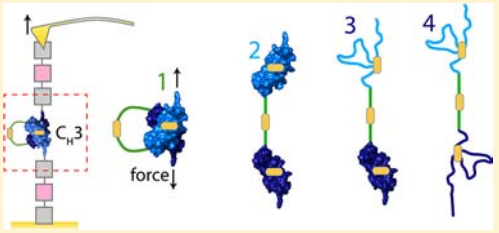

INTRODUCTION

Antibodies are proteins that have evolved to recognize and bind a vast number of different target molecules. They constitute a vital part of the antibody-mediated humoral immune response providing protection against infections and foreign antigens and are widely used as therapeutic agents and in biotechnology. The prevalent antibody, immunoglobulin G (IgG), is a heterotetramer (Figure 1A) consisting of two identical light and two identical heavy chains composed of 2 or 4 domains of the Ig (immunoglobulin) fold, respectively. Each of these Ig domains comprises ≈100 amino acids arranged into two opposing β-sheets (Figure 1B). A buried disulfide bridge connects the two halves of this β-sandwich, which, if formed, increases the stability of these domains significantly.[1]

Based on proteolytic fragments, IgGs can be divided into two Fab (antigen-binding) and one Fc (crystallizable) segments. Fc, the homodimer of heavy chain domains C_H2 and C_H3, forms the stem of the antibody and is responsible for triggering the antibody-mediated immune response. The antigen-binding site is located at the N-terminal tip of Fab, which consists of the light chain and heavy chain domains V_H and C_H1. A hinge region connects the two Fab fragments to Fc. The hinge region is highly flexible and allows the two Fabs to adopt a wide range of conformations relative to Fc, making the antibody asymmetric. The large conformational freedom of the Fabs, which has been observed in crystal structures[2,3] by electron microscopy[4] and by small-angle X-ray scattering,[5] can extend the effective binding range of the antibody protein.[4] Deletions or mutations in the hinge region restrict this conformational freedom and result in antibodies that adopt a symmetrical T- or Y-shaped conformation.[6]

Antibody folding and assembly is an intricate process involving many steps and several layers of quality control to ensure the production of functional antibody molecules.[7] Stability of the assembled antibody protein is essential for its role in vivo, especially considering that antibodies have to function in the harsh extracellular environment, sometimes at high dilution. The complex antibody structure is stabilized by interactions between Ig domains (the C_H3 dimer and C_L-C_H1) in addition to disulfide bridges linking the heavy chains between domains C_H1 and C_H2 in the hinge region and the light chain and the heavy chain between the C_L C-terminus and C_H1.

The noncovalent interaction between the C_H3 domains (Figure 1B) is the first step of antibody assembly and the main interaction stabilizing the two heavy chains, which in turn provide the molecular scaffold for the subsequent steps of the assembly of the native antibody.[7] Dissociation of C_H3 is the rate-limiting step for Fab-arm exchange, observed in IgG type 4 antibodies. In this process, the antibody dissociates into two half-molecules each consisting of a light and a heavy chain, and half-molecules from two different antibodies can reassemble to form heterodimeric bispecific antibodies,[8,9] which are of particular interest for antibody therapy.

Dimeric C_H3 is the simplest example of Ig domain folding and assembly found in antibodies and can therefore serve as a model system for the protein−protein interactions that govern antibody

Received: May 21, 2013
Published: September 10, 2013

   dx.doi.org/10.1021/ja405076j | J. Am. Chem. Soc. 2013, 135, 15085−15091

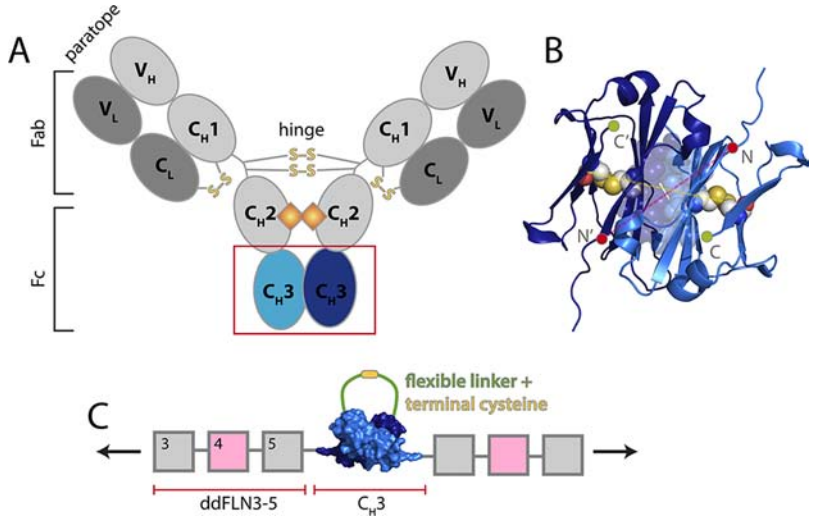

Figure 1. Antibody architecture and structure of C_H3. (A) Domain layout of an IgG-type antibody. Interchain disulfide bridges are shown in yellow, and oligosaccharides attached to antibody domain C_H2 are shown as orange squares. The two major fragments, Fab and Fc, as well as the antigen-binding paratope formed by the variable domains V_L and V_H are highlighted. (B) High-resolution structure of dimeric C_H3 (PDB ID: 1CQK) from the murine antibody MAK33. The two intradomain disulfide bridges and the residues forming the domain−domain interface are shown as space-filling amino acids. N- (red circles) and C- (green circles) termini are highlighted in the structure, the direction of force application to the complex is indicated as a red line, and the direction of the disulfide bridges is shown in yellow. (C) Molecular architecture of the filamin-C_H3 chimera. Filamin domain ddFLN4, which unfolds via an intermediate state, is highlighted in pink. The flexible linker carrying a terminal cysteine fused to the C_H3 C terminus is shown in green. The arrows indicate the direction of force application during stretching.

stability. Bulk chemical unfolding studies have shown that for C_H3 the disulfide bridge is not required for folding and association but that reduced C_H3 has a lower thermodynamic stability.[10] Here, we use single-molecule force spectroscopy to investigate the dissociation mechanics of the C_H3 dimer and, in particular, the influence of its intradomain disulfide bridge on its dissociation pathway.

EXPERIMENTAL SECTION

The C_H3 domain from the murine antibody MAK33, an IgG1, (residues 343−450)[11] was fused to the C-terminus of Ig-domains 3-5 of *Dictyostelium discoideum* filamin (ddFLN3-5),[12] which carried an N-terminal 6x His tag. To covalently connect the two C_H3 subunits, a flexible linker of 10 amino acids (glycine/serine) with a terminal cysteine was fused to the C-terminus of C_H3 by PCR (sequence SGGSGSGGSGC). Protein expression was carried out in BL21(DE3) Codon Plus(RIL) cells and the soluble filamin-C_H3 fusion protein was purified by nickel-affinity chromatography followed by size-exclusion chromatography using a Superdex200 column in PBS. Purity of the protein and formation of the interchain C-terminal disulfide bridge was assessed by nonreducing SDS-PAGE. Directly after purification, the interchain disulfide bridge had formed in ∼50% of the sample (Figure S3).

Single-molecule force spectroscopy was carried out using a custom-built atomic force microscope at ambient temperature. In all experiments, gold-coated cantilevers (Biolever type A or B, Olympus) with a nominal spring constant of 30 or 6 pN/nm were used. In a typical experiment, the purified protein was applied to a freshly activated Ni-NTA surface and force−extension traces were recorded at a pulling velocity of 1 μm/s. Data were acquired at a sampling rate of 20 kHz with a digital filter set to 10 kHz. Upon recording, traces were screened for the well-characterized unfolding signature of ddFLN domains. These traces were later inspected for additional reproducible features that appeared in addition to the unfolding signature of ddFLN. Contour length increases (ΔL) were determined using the interpolation formula of the WLC model as introduced by Bustamante et al.[13] with a fixed persistence length of 0.5 nm. Contour length increases were used to determine the number of amino acids involved in an unfolding transition via

$$\Delta L = n \cdot d_{aa} - d_{state2} + d_{state1} \quad (1)$$

Here, d_{state2} and d_{state1} denote the distance between the points of force application in the intermediate and the native state, respectively, and d_{aa} is the contour length increase per amino acid, which has been determined to be d_{aa} = 0.365 ± 0.002 nm for our instrument at a persistence length of 0.5 nm.[14] Loading rates were estimated by linear fits to the force vs time trace directly before an unfolding event. Unloaded lifetimes and transition-state positions were determined by Monte Carlo simulations taking into account cantilever relaxation and the length of unfolded peptide before unfolding as described.[15]

RESULTS

The protein construct used in this study is outlined in Figure 1C. The N-terminus of a C_H3 domain was fused to three Ig domains from ddFLN3-5 (gray and pink squares), which serve as handles for connecting C_H3 to the surface and the cantilever of the AFM instrument. In this geometry, force will be applied to the N-termini of the C_H3 homodimer, which is the attachment site for the C_H2 domain in the authentic antibody heavy chain. The force will act roughly at 45° to the direction of the β-strands and perpendicular to the disulfide bridges (compare Figure 1B). A 10 amino acid glycine/serine linker with a terminal cysteine was added to the C-terminus of each C_H3 domain (green line in Figure 1C). A disulfide bond can form between two of these linkers in the C_H3 dimer (yellow line in Figure 1C), and this covalent tether will connect the two ddFLN-C_H3 polypeptide chains even after C_H3 dissociation. Flexible tethers fused to the termini of protein complexes have been successfully employed to study protein−protein interactions using single-molecule force spectroscopy in previous studies.[16−21]

In a typical experiment using this protein chimera, all force−extension traces were screened for the unfolding signature of ddFLN3-5 consisting of evenly spaced ≈32 nm peaks at forces between 50 and 150 pN (gray peaks in Figure 2B−D);[12] traces lacking these features were discarded. Among the three filamin domains, ddFLN4 shows a unique double peak during mechanical unfolding stemming from an intermediate state

dx.doi.org/10.1021/ja405076j | J. Am. Chem. Soc. 2013, 135, 15085−15091

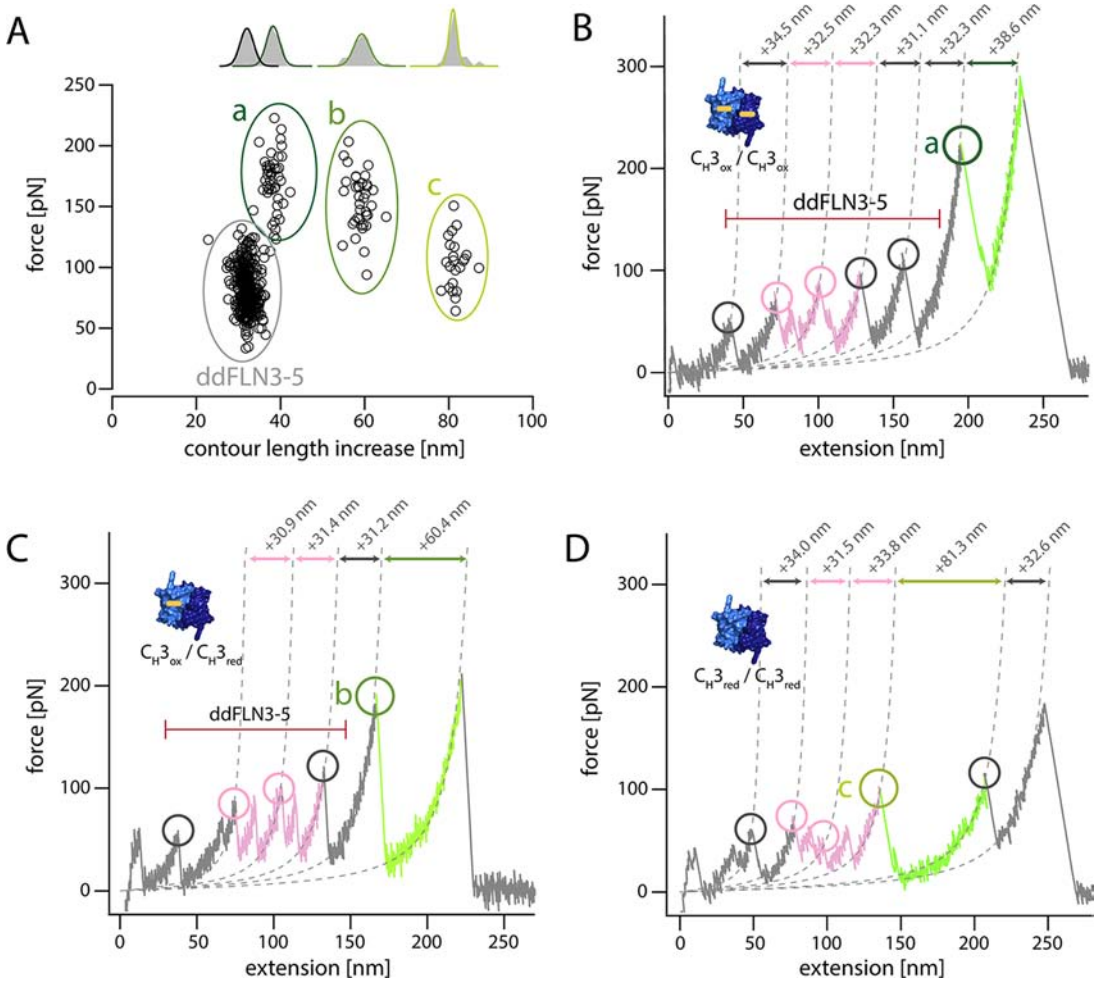

Figure 2. Mechanical dissociation of C_H3. (A) Scatter plot of dissociation force vs contour length increase (ΔL) for the dimeric filamin-C_H3 chimera. Four populations emerge from the scatter plot (circles). Contour length distributions with Gaussian fits to the data are indicated above the four populations. Representative force–extension traces for the dissociation of fully oxidized C_H3_{ox}/C_H3_{ox} (B), mixed C_H3_{ox}/C_H3_{red} (C), and fully reduced C_H3_{red}/C_H3_{red} (D). A green circle marks the dissociation of C_H3; the green segment of the trace represents the stretching of the flexible C-terminal linker and unfolded C_H3 domains. Filamin domain ddFLN4 unfolding events, which show a characteristic double peak, are indicated in pink, ddFLN3 and ddFLN5 unfolding peaks are marked with gray circles. Broken gray lines represent WLC fits, from which the contour length of each state are determined. Contour length increases are displayed above the traces.

that is populated on the unfolding pathway (Figure 2B–D, pink double peaks).[12] Since C_H3 is flanked by two ddFLN4 domains in the dimeric protein construct, the presence of two ddFLN4 unfolding events in a single unfolding trace indicates that the protein chain was attached to the AFM instrument N-terminal of ddFLN4 and that the C_H3 dimer interface was exposed to force. Consequently, traces showing two unfolding events of ddFLN4 were selected for further analysis.

Unfolding forces and the increase in contour length upon unfolding (ΔL) were determined using worm-like chain (WLC) fits to the unfolding peaks (gray broken lines in Figure 2B-D). In the case of ddFLN4, WLC fits were only done for the first unfolding event, while the intermediate state was omitted during this analysis. A scatter plot of unfolding force versus ΔL is shown in Figure 2A. The majority of events (Figure 2A, gray circle) displays unfolding forces between 40 and 130 pN and a narrowly distributed ΔL = 32.0 ± 0.2 nm (mean ± S.E.M, n = 323), in good agreement with the previously reported value of 31.5 nm for ddFLN3-5.[12] In addition to these events, which stem from the handle domains fused to C_H3, the scatter plot shows three additional populations, with ΔL clearly larger than that observed for ddFLN3-5 and with higher unfolding forces [dark-green (a), green (b) and light-green (c) populations in the scatter plot]. Representative force–extension traces corresponding to populations a–c are shown in Figure 2B–D. We attribute these additional unfolding populations to the dissociation and unfolding of C_H3.

How can the different classes of events be rationalized using the geometry of the protein construct and the structure of C_H3? Regardless of the precise unfolding pathway, each unfolding event will originate from the folded C_H3 dimer (tethered by the C-terminal linkers) and end up with two separated and completely unfolded C_H3 domains. Dissociation of the dimer will stretch out the flexible, C-terminal linker and reorient the two C_H3 domains along the direction of the applied force (compare cartoons in Figure 3A–D). Assuming a contour length increase per amino acid of 0.365 nm[14] and taking into account the dimensions of C_H3,[11] this results in an expected ΔL = 13.8 nm. [For this calculation, the folded part of C_H3 consists of residues Pro7 to Ser103 of the crystal structure (PDB ID 1CQK) of C_H3. The effective length of the C terminal linker is n_{aa} = 16 residues, consisting of 4 terminal amino acids of C_H3 that do not

dx.doi.org/10.1021/ja405076j | J. Am. Chem. Soc. 2013, 135, 15085–15091

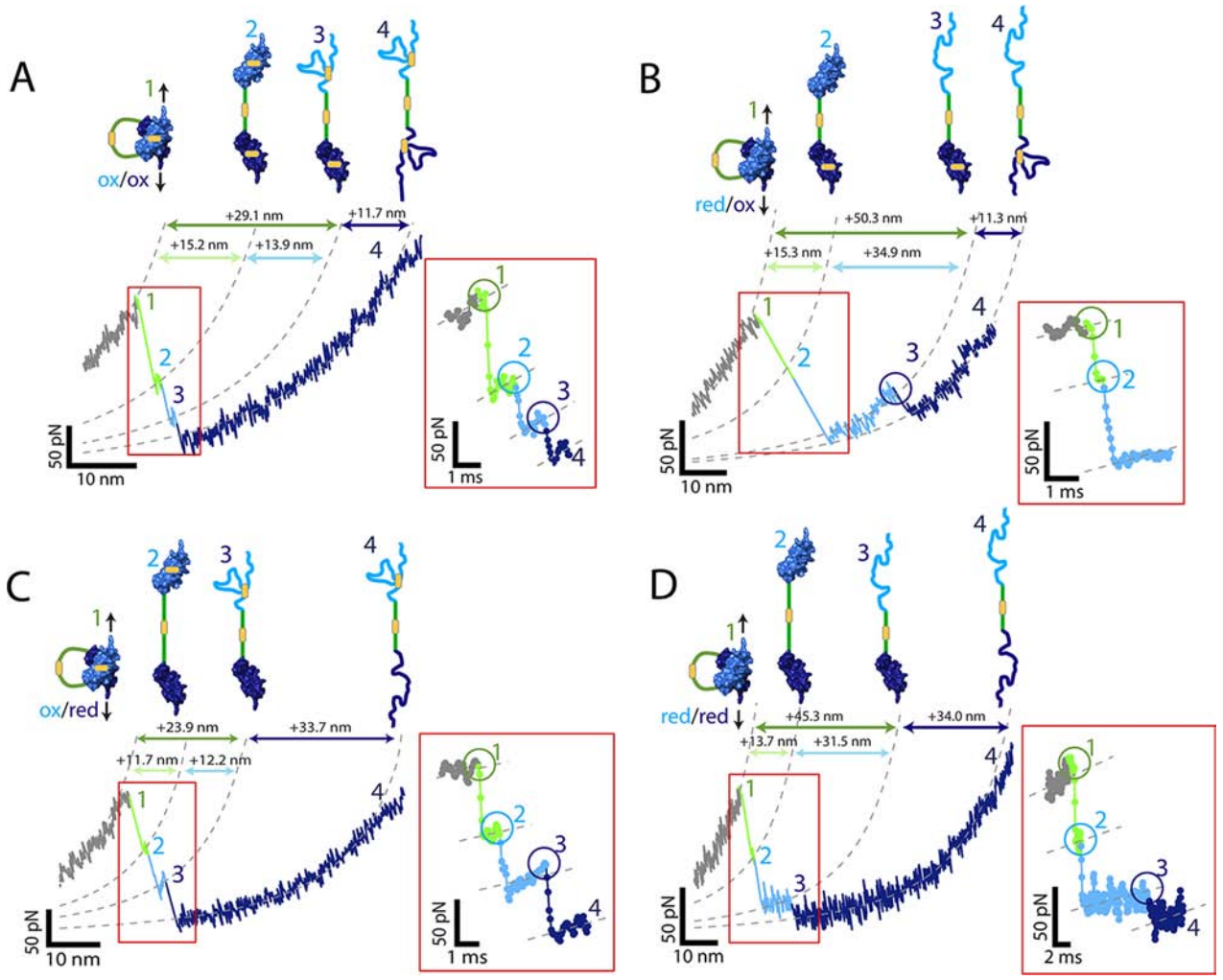

Figure 3. Detailed dissociation pathway of C_H3 under different redox conditions: (A) C_H3_{ox}/C_H3_{ox}, (B) mixed C_H3_{ox}/C_H3_{red} with the reduced monomer C_H3_{red} unfolding first, (C) mixed C_H3_{ox}/C_H3_{red} with the oxidized monomer C_H3_{ox} unfolding first, and (D) fully reduced C_H3_{red}/C_H3_{red}. In all four traces, event 1 (green) marks dissociation, event 2 (light blue) unfolding of the first monomer, event 3 (dark blue) unfolding of the second monomer, and 4 (violet) the stretching of fully unfolded C_H3 polypeptide chain. Structural models corresponding to these four events are shown above the traces, with disulfide bridges indicated by a yellow bar. The boxed part of each trace is shown as force vs time in the right part of each panel, with unfolding/dissociation events marked by circles.

participate in the Ig sandwich, the engineered 10 amino acid glycine-serine linker, and the terminal cysteine. $\Delta L = 2 \cdot n_{aa} \cdot 0.365 - d_{C_H3dimer} + 2 \cdot d_{C_H3monomer} + d_{SS}$. Here, $d_{C_H3dimer}$ is the distance between the points of force application in dimeric C_H3 (2.9 nm between Pro7 and Pro7), $d_{C_H3monomer}$ is the N−C-terminal distance of a C_H3 monomer (2.2 nm), and d_{ss} is the distance between 2 Cα atoms in the terminal disulfide bond (0.6 nm).] For each C_H3 domain, only the amino acids outside the native disulfide bridge between residues Cys28 and Cys86 can contribute to the contour length increase, resulting in an expected ΔL = 12.3 nm for stretching 38 amino acids of each domain. In total, dissociation and unfolding of a C_H3 dimer should hence lead to an expected ΔL = 38.4 nm, which nicely corresponds to population (a) observed in the scatter plot in Figure 2A [measured value: 38.2 ± 0.4 nm (mean ± S.E.M, n = 55), compare Figure 2B for a representative force−extension trace].

While the internal disulfide bridge is considered a hallmark of antibody Ig domains, it has been shown that the Ig fold can also form in its absence.[1] In our study, the protein was expressed in the *E. coli* cytosol and purified without any added oxidants. Consequently, it is conceivable that the internal disulfide bridge in C_H3 was not formed in all protein molecules in the sample. The presence or absence of the internal disulfide bridge, however, has direct consequences for ΔL after dissociation, since in the reduced state all 96 amino acids of a C_H3 monomer can be stretched, as opposed to only 38 amino acids in oxidized C_H3. Unfolding of a reduced C_H3 monomer thus leads to a longer contour length increase of 32.8 nm. Accordingly, the two additional populations observed in the scatter plot in Figure 2A stem from a mixed oxidized/reduced C_H3 dimer ($C_H3_{ox/red}$, expected ΔL = 58.9 nm) with a measured ΔL = 59.3 ± 0.6 nm (mean ± S.E.M, n = 45) (population (b), curve in Figure 2C) and the fully reduced C_H3 dimer ($C_H3_{red/red}$, expected ΔL = 80.0 nm) with ΔL = 81.0 ± 0.4 nm (mean ± S.E.M, n = 29) (population (c), curve in Figure 2D). Our single-molecule assay thus allows us to differentiate between different redox states of a protein in an inhomogeneous sample by their difference in contour length increase after unfolding (ΔL).

In this inhomogeneous sample, initially only half the domains were in the fully oxidized state. Spontaneous oxidation of C_H3

dx.doi.org/10.1021/ja405076j | J. Am. Chem. Soc. 2013, 135, 15085−15091

occurred on a time scale of weeks in the absence of added oxidants, as judged from the number of unfolding traces showing the dissociation of $C_H3_{ox/ox}$, $C_H3_{red/ox}$, and $C_H3_{red/red}$ at different points of time (Figure S1). Slow spontaneous disulfide bond formation in dimeric C_H3 has been observed before[10,22] and is likely because C_H3 has to both dissociate and unfold for oxidation to take place.

Closer inspection of the force−extension trace revealed additional features after C_H3 dissociation. In the case of $C_H3_{ox/ox}$ (Figure 3A), the highest force peak (green circle in Figure 3A) represents the dissociation of the dimer with a length increase of ≈15 nm, after which the unfolding of two separated monomers can be observed in two distinct steps (light- and dark-blue circle in Figure 3A, length increase histograms in Figure S2). Stretching the C-terminal linker by dissociating C_H3 (transition 1 to 2) results in only a short length increase, and consequently the force remains high (>100 pN) after dissociation. According to Bell, the lifetime of a bond decreases exponentially with the applied force.[23] Hence when the two monomers are exposed to a high force directly after they are formed in this experiment, they are only short-lived. A zoom into the data (red box), which shows individual data points of the unfolding trace at 20 kHz sampling frequency, clearly shows that the cantilever dwells at well-defined positions of approximately equal spacing during cantilever relaxation after the first unfolding peak. The lifetime of the first intermediate state (two C_H3_{ox} monomers, light-blue circle) is at the detection limit of our instrument and could not be reliably detected in all traces. After the first C_H3_{ox} monomer is unfolded, however, the force drops down further (below 100 pN, dark-blue circle), resulting in a longer lifetime and in turn more reliable detection for the remaining second C_H3_{ox} monomer. Accordingly, we only determined ΔL for the unfolding of the second monomer (transition 3 to 4 in Figure 3A), which at $\Delta L = 12.8 \pm 0.5$ nm corresponds well to the expected value for unfolding a single oxidized C_H3_{ox} domain (expected value 12.3 nm, also compare histograms in Figure S2). A similar behavior was observed in fully reduced $C_H3_{red/red}$ (Figure 3D): A short length increase (dissociation, transition 1 to 2) was followed by two unfolding events of equal length (transitions 2 to 3 and 3 to 4), which represent the unfolding of the two reduced C_H3_{red} monomers. The unfolding of the second C_H3_{red} monomer, which again can be detected with greater reliability, results in $\Delta L = 30.9 \pm 0.6$ nm, again matching the expected value (33 nm) within the resolution of the experiment (Figure S2). For the mixed dimer $C_H3_{red/ox}$ two classes of curves were observed: In the majority of unfolding traces (39 out of 45), dissociation (transition 1 to 2 in Figure 3B) was followed by a long length increase (transition 2 to 3 in Figure 3B) of ≈32 nm and a subsequent shorter event ($\Delta L = 11.6 \pm 1.3$ nm). In these curves, the reduced C_H3_{red} monomer unfolded first, followed by the oxidized C_H3_{ox} monomer in a second step. In some curves (6 out of 45), however, the sequence of events was reversed, and unfolding of the oxidized monomer C_H3_{ox} (transition 2 to 3 in Figure 3C) occurred before unfolding of C_H3_{red} (transition 3 to 4 in Figure 3C, $\Delta L = 30.1 \pm 2.2$ nm).

How does the reduction of one or both disulfide bonds in C_H3 affect the mechanical stability of the dimer? Histograms of the dissociation force in the three different oxidation states are shown in Figure 4. $C_H3_{ox/ox}$ dissociates at 174 ± 5 pN, $C_H3_{red/ox}$ at 152 ± 5 pN, and $C_H3_{red/red}$ at 117 ± 5 pN. We used Monte Carlo simulations to extract dissociation rates in the absence of force (k_{off}) and the position of the transition state in the energy landscape (Δx) from the dissociation force distributions (black lines in Figure 4, simulation parameters are detailed in the figure legend). Strikingly, reduction of the protein increases the dissociation rate by a factor of 4−5 for each reduced disulfide bond while leaving the transition-state position Δx unaffected. To gain additional insight into the contributions of the individual C_H3 subunits, we measured the lifetime of the monomeric C_H3_{ox} (inset in Figure 4) in unfolding traces starting from the fully oxidized dimer (event 3 in Figure 3A), since for the dissociation of $C_H3_{ox/ox}$ most data were available. During the short lifetime of monomeric C_H3_{ox}, the force remains almost constant, making the lifetime a better parameter to analyze than the unfolding force. The lifetime distribution was reproduced using a Monte Carlo simulation taking into account cantilever relaxation following the preceding dissociation events (black line in the inset of Figure 4). The simulation yielded a dissociation rate of $k_{off} = 3\ s^{-1}$ and a transition-state position of $\Delta x = 2.5$ Å. For the reduced monomer C_H3_{red}, data were not sufficient for the direct determination of kinetic parameters.

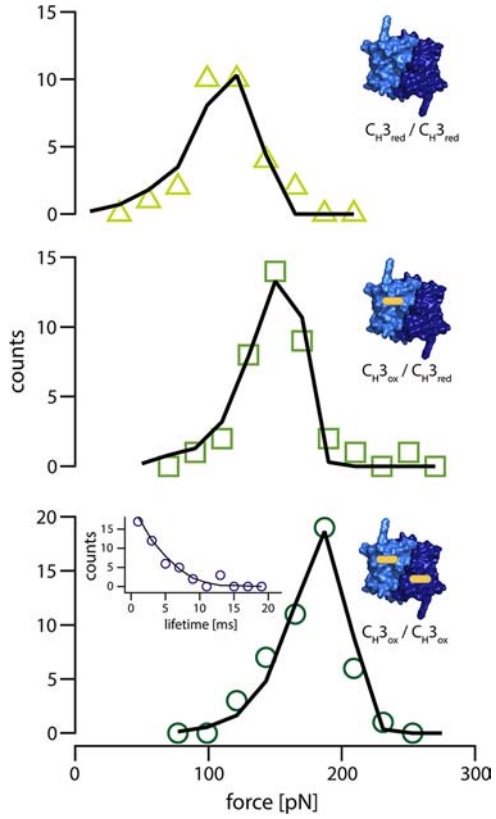

Figure 4. Dissociation force distributions for C_H3_{red}/C_H3_{red} (top), C_H3_{ox}/C_H3_{red} (center), and C_H3_{ox}/C_H3_{ox} (bottom), with simulated distributions indicated by black lines. Parameters for Monte Carlo unfolding simulations were $\Delta x = 2.5$ Å, $k_{off} = 0.2\ s^{-1}$ for C_H3_{red}/C_H3_{red}, $\Delta x = 2.3$ Å, $k_{off} = 0.05\ s^{-1}$ for C_H3_{ox}/C_H3_{red}, and $\Delta x = 2.4$ Å, $k_{off} = 0.01\ s^{-1}$ for C_H3_{ox}/C_H3_{ox}. The inset shows the lifetime distribution of a single C_H3_{ox} monomer at constant force after dissociation, with the black line indicating the results of a Monte Carlo simulation with $\Delta x = 2.5$ Å, $k_{off} = 3\ s^{-1}$.

DISCUSSION

In this study, we have used single-molecule force spectroscopy to reveal the mechanical makeup of C_H3 in detail. Using a heterogeneous sample containing C_H3 in different oxidation states, we distinguish different C_H3 redox states by their contour length increase. In particular, we could determine the stability of

dx.doi.org/10.1021/ja405076j | J. Am. Chem. Soc. 2013, 135, 15085−15091

mixed C_H3_{ox}/C_H3_{red}, which is not easily accessible in conventional bulk stability measurements. Single-molecule force spectroscopy is uniquely suited to determine the stability of proteins or protein complexes involving disulfide bonds, since the oxidation state of the protein is directly reported via the contour length increase after unfolding ΔL. Accordingly, single-molecule force spectroscopy has been used to directly observe disulfide-bond reduction[24] or protein disulfide-bond formation.[25]

With a mean dissociation force of 174 ± 5 pN, oxidized C_H3 has a remarkably high mechanical stability, surpassing typical antibody−antigen interactions by about a factor of 3[26] at similar loading rates (average loading rates ranged from 5570 pN/s for C_H3_{ox}/C_H3_{ox}, over 5470 pN/s for C_H3_{ox}/C_H3_{red}, to 3200 pN/s for C_H3_{red}/C_H3_{red}). Intriguingly, C_H3 is also more stable than several homo- or heterodimeric protein complexes found in muscle, such as the myomesin myo13 homodimer (137 pN)[18] or the complex between titin domain M10 and obscurin domain 1 (29 pN),[19] whose physiological role is considered to involve bearing mechanical load. The high-affinity cohesion−dockerin complex, which anchors cellulosomes on the bacterial cell surface, ruptures at around 120 pN,[27] the dimeric α-crystallin domain of the small heat shock protein Hsp16.5 dissociates at 180 pN,[21] and the much larger ternary titin-telethonin complex can withstand up to 700 pN.[28] With the exception of cohesion−dockerin, these complexes consist of two or more domains of the immunoglobulin fold, as it is the case for C_H3. In contrast to C_H3, however, association in these complexes involves interdomain β-sheets[29] between the Ig domains, with an extensive network of hydrogen bonds between the subunits. Shearing of load-bearing β-strands requires breaking several hydrogen bonds simultaneously, and this 'mechanical clamp' motif is considered to be responsible for the high mechanical stability found in titin I27,[30] ubiquitin,[31] or scaffoldin.[32] C_H3 is lacking this 'mechanical clamp', and the dimer is primarily stabilized by hydrophobic interactions involving 16 residues at the domain interface,[11] with the main interaction formed by a patch of only five residues.[33] Our data show that these hydrophobic interactions form a high affinity protein−protein interface that is also highly stable mechanically, consistent with a dissociation constant of $<10^{-10}$ M^{-1}.[34]

The stabilizing effect of disulfide bonds on proteins in general[35] and Ig domains in particular[1] has long been realized. Disulfide bonds restrict the conformational space accessible to the unfolded state, thereby lowering its entropy and favoring the native state.[35] In addition, disulfide bonds have been shown to accelerate the formation of on-pathway folding intermediates in Ig domains.[36] Reduced C_H3 showed a roughly 8-fold lower thermodynamic stability against chemical denaturation and an ≈ 3-fold higher unfolding rate compared to the fully oxidized protein in bulk unfolding experiments.[11]

In contrast to chemical denaturation, force acts locally on a protein structure.[37] An increase in mechanical stability by disulfide bonding hence would only be expected if formation of the disulfide bridge strengthens load-bearing structures within the protein. Disulfide bridges thus do not a priori result in an increase of mechanical stability, and in fact, previous mechanical unfolding experiments with Ig domains that contained native[38] or engineered[39] buried disulfide bridges reported a decrease of mechanical stability when the disulfide bridge was present. In the case of C_H3, however, we observe that the presence of the disulfide bridges significantly increases the dissociation force from 117 to 174 pN. For C_H3, the disulfide bridge evidently has a structural role and stabilizes the dimeric native state, which has been proposed before.[22] The stability of the C_H3 dimer with one disulfide bond removed falls between the fully oxidized and the fully reduced complex, and the effect of disulfide bond reduction is additive, as illustrated by the 5-fold increase in unfolding rate per disulfide bond removed. This points to a rearrangement of the dimerization interface, with some but not all interactions broken when the protein is partially reduced. Far-UV spectroscopy of reduced C_H3 has suggested that the C_H3 monomer forms a more compact structure when the disulfide bridge between the two β-sheets of one Ig domain is removed.[10] Upon reduction of one disulfide bond, this kind of structural change would perturb only one side of the domain−domain interface, which could explain the additive stabilization effect of the disulfide bonds we observe in our mechanical measurements. The disulfide bridge thus helps mold the high-affinity interface in C_H3.

In our experiments, regardless of redox state, C_H3 dissociation always proceeded from the fully folded dimer to two folded monomers, which subsequently unfold in two steps. With an unloaded lifetime of ≈ 300 ms, folded monomeric C_H3_{ox} is short-lived, which explains why no monomeric species have been observed during bulk unfolding experiments of C_H3.[10,11] While we could not directly determine an unfolding rate for reduced C_H3_{red}, we can estimate the unfolding rate from the unfolding data of the mixed C_H3_{ox}/C_H3_{red} dimer: After the dissociation of C_H3_{ox}/C_H3_{red}, an oxidized C_H3_{ox} and a reduced C_H3_{red} are formed. We find that in one out of seven dissociation traces, C_H3_{ox} will unfold first, while in the remaining cases C_H3_{red} unfolds first. Assuming the same transition state position for C_H3_{ox} and C_H3_{red}, this indicates a 7-fold lower lifetime (≈ 40 ms) for C_H3_{red}.

C_H3 dimerization is the first step of antibody assembly, and the C_H3 dimer is the main interaction stabilizing antibody heavy chains.[7] Consequently, the stability of C_H3 is essential for proper antibody function. Although antibodies and therefore C_H3 do not perform a primarily mechanical role in vivo, one can imagine scenarios where the C_H3 dimer is exposed to strain, for example, through hydrodynamic flow when bound to cell surface proteins.[40] Destabilization of C_H3 by strain resulting from binding two spatially separated epitopes, for example, on a cell surface, has been proposed as a mechanism facilitating Fab-arm exchange observed in IgG4 antibodies.[8,41] In the absence of hinge disulfide bonds, strain would be transmitted from the antigen binding sites through the heavy chain to the N-termini of C_H3, a situation that is mimicked by our experimental geometry. Furthermore, antibodies are widely used as molecular anchors in mechanical assays. In this context, our data provide a limit on how much force a single antibody can bear and how this force is affected by redox conditions. The stable C_H3 dimer can ensure antibody integrity even when disulfide bridges are broken, for example, under reducing conditions. C_H3 therefore provides a fastener that prevents antibody dissociation even under harsh extracellular conditions or in highly dilute concentrations.

■ CONCLUSION

In summary, our results reveal C_H3 as a mechanically very stable dimer whose stability is strongly dependent on its disulfide bridge. This is especially relevant considering that incomplete disulfide bond formation is commonly observed in full-length antibodies purified from hybridoma cells, with C_H3 showing up to 10% of missing disulfide bonds, the highest percentage of all antibody Ig domains.[42] Our data demonstrate that even in the fully reduced but dimeric state, C_H3 can still withstand significant

mechanical load. Monomeric C_H3, on the other hand, is mechanically labile, indicating that this domain was evolved to function as a stable dimer.

■ ASSOCIATED CONTENT

Supporting Information

Time course of the relative populations of the different oxidation states of C_H3, additional contour length increases histograms, and reducing/nonreducing SDS-PAGE of the cross-linked sample. This material is available free of charge via the Internet at http://pubs.acs.org.

■ AUTHOR INFORMATION

Corresponding Author

morten.bertz@ph.tum.de; morten.bertz@aoni.waseda.jp

Present Address

[‖]Department of Physics, Faculty of Science and Engineering, Waseda University, 3-4-1 Okubo, Shinjuku-ku, Tokyo 169-8555, Japan

Notes

The authors declare no competing financial interest.

■ ACKNOWLEDGMENTS

We wish to thank Kazuhiko Kinosita Jr. for discussions and helpful comments on the manuscript. This work was supported by Deutsche Forschungsgemeinschaft through grant SFB 863 to M.R. and J.B. and through a DFG grant to J.B.

■ REFERENCES

(1) Goto, Y.; Hamaguchi, K. *J. Biochem.* **1979**, *86*, 1433−1441.
(2) Harris, L. J.; Skaletsky, E.; McPherson, A. *J. Mol. Biol.* **1998**, *275*, 861−872.
(3) Saphire, E. O.; Stanfield, R. L.; Max Crispin, M. D.; Parren, P. W. H. I.; Rudd, P. M.; Dwek, R. A.; Burton, D. R.; Wilson, I. A. *J. Mol. Biol.* **2002**, *319*, 9−18.
(4) Sandin, S.; Öfverstedt, L.-G.; Wikström, A.-C.; Wrange, Ö.; Skoglund, U. *Structure* **2004**, *12*, 409−415.
(5) Lilyestrom, W. G.; Shire, S. J.; Scherer, T. M. *J. Phys. Chem. B* **2012**, *116*, 9611−9618.
(6) Silverton, E. W. E.; Navia, M. A. M.; Davies, D. R. D. *Proc. Natl. Acad. Sci. U.S.A.* **1977**, *74*, 5140−5144.
(7) Feige, M. J.; Hendershot, L. M.; Buchner, J. *Trends Biochem. Sci.* **2010**, *35*, 10−10.
(8) Rispens, T.; Ooijevaar-de Heer, P.; Bende, O.; Aalberse, R. C. *J. Am. Chem. Soc.* **2011**, *133*, 10302−10311.
(9) van der Neut Kolfschoten, M.; Schuurman, J.; Losen, M.; Bleeker, W. K.; Martínez-Martínez, P.; Vermeulen, E.; Bleker, den, T. H.; Wiegman, L.; Vink, T.; Aarden, L. A. *Science* **2007**, *317*, 1554−1557.
(10) Thies, M. J.; Talamo, F.; Mayer, M.; Bell, S.; Ruoppolo, M.; Marino, G.; Buchner, J. *J. Mol. Biol.* **2002**, *319*, 1267−1277.
(11) Thies, M. J.; Mayer, J.; Augustine, J. G.; Frederick, C. A.; Lilie, H.; Buchner, J. *J. Mol. Biol.* **1999**, *293*, 67−79.
(12) Schwaiger, I.; Kardinal, A.; Schleicher, M.; Noegel, A. A.; Rief, M. *Nat. Struct. Mol. Biol.* **2004**, *11*, 81−85.
(13) Bustamante, C.; Marko, J. F.; Siggia, E. D.; Smith, S. *Science* **1994**, *265*, 1599−1600.
(14) Dietz, H.; Rief, M. *Proc. Natl. Acad. Sci. U.S.A.* **2006**, *103*, 1244−1247.
(15) Rief, M.; Fernandez, J. M.; Gaub, H. E. *Phys. Rev. Lett.* **1998**, *81*, 4764−4767.
(16) Junker, J. P.; Rief, M. *Proc. Natl. Acad. Sci. U.S.A.* **2009**, *106*, 14361−14366.
(17) Junker, J. P.; Ziegler, F.; Rief, M. *Science* **2009**, *323*, 633−637.
(18) Berkemeier, F.; Bertz, M.; Xiao, S.; Pinotsis, N.; Wilmanns, M.; Grater, F.; Rief, M. *Proc. Natl. Acad. Sci. U.S.A.* **2011**, *108*, 14139−14144.
(19) Pernigo, S.; Fukuzawa, A.; Bertz, M.; Holt, M.; Rief, M.; Steiner, R. A.; Gautel, M. *Proc. Natl. Acad. Sci. U.S.A.* **2010**, *107*, 2908−2913.
(20) Kim, J.; Zhang, C.-Z.; Zhang, X.; Springer, T. A. *Nature* **2010**, *466*, 992−995.
(21) Bertz, M.; Chen, J.; Feige, M. J.; Franzmann, T. M.; Buchner, J.; Rief, M. *J. Mol. Biol.* **2010**, *400*, 1046−1056.
(22) McAuley, A.; Jacob, J.; Kolvenbach, C. G.; Westland, K.; Lee, H. J.; Brych, S. R.; Rehder, D.; Kleemann, G. R.; Brems, D. N.; Matsumura, M. *Protein Sci.* **2008**, *17*, 95−106.
(23) Bell, G. I. *Science* **1978**, *200*, 618−627.
(24) Wiita, A. P.; Perez-Jimenez, R.; Walther, K. A.; Grater, F.; Berne, B. J.; Holmgren, A.; Sanchez-Ruiz, J. M.; Fernandez, J. M. *Nature* **2007**, *450*, 124−127.
(25) Kosuri, P.; Alegre-Cebollada, J.; Feng, J.; Kaplan, A.; Inglés-Prieto, A.; Badilla, C. L.; Stockwell, B. R.; Sanchez-Ruiz, J. M.; Holmgren, A.; Fernández, J. M. *Cell* **2012**, *151*, 794−806.
(26) Morfill, J.; Blank, K.; Zahnd, C.; Luginbuhl, B.; Kuhner, F.; Gottschalk, K. E.; Pluckthun, A.; Gaub, H. E. *Biophys. J.* **2007**, *93*, 3583−3590.
(27) Stahl, S. W.; Nash, M. A.; Fried, D. B.; Slutzki, M.; Barak, Y.; Bayer, E. A.; Gaub, H. E. *Proc. Natl. Acad. Sci. U.S.A.* **2012**, *109*, 20431−20436.
(28) Bertz, M.; Wilmanns, M.; Rief, M. *Proc. Natl. Acad. Sci. U.S.A.* **2009**, *106*, 133307−133310.
(29) Pinotsis, N.; Abrusci, P.; Djinovic Carugo, K.; Wilmanns, M. *Trends Biochem. Sci.* **2009**, *34*, 33−39.
(30) Lu, Schulten *Chem. Phys.* **1999**, *247*, 13−13.
(31) Carrion-Vazquez, M.; Li, H.; Lu, H.; Marszalek, P. E.; Oberhauser, A. F.; Fernandez, J. M. *Nat. Struct. Biol.* **2003**, *10*, 738−743.
(32) Valbuena, A.; Oroz, J.; Hervas, R.; Vera, A. M.; Rodriguez, D.; Menendez, M.; Sulkowska, J. I.; Cieplak, M.; Carrion-Vazquez, M. *Proc. Natl. Acad. Sci. U.S.A.* **2009**, *106*, 13791−13796.
(33) Dall'Acqua, W.; Simon, A. L.; Mulkerrin, M. G.; Carter, P. *Biochemistry* **1998**, *37*, 9266−9273.
(34) Isenman, D. E.; Lancet, D.; Pecht, I. *Biochemistry* **1979**, *18*, 3327−3336.
(35) Pace, C. N.; Grimsley, G. R.; Thomson, J. A.; Barnett, B. J. *J. Biol. Chem.* **1988**, *263*, 11820−11825.
(36) Feige, M. J.; Hagn, F.; Esser, J.; Kessler, H.; Buchner, J. *J. Mol. Biol.* **2007**, *365*, 1232−1244.
(37) Dietz, H.; Berkemeier, F.; Bertz, M.; Rief, M. *Proc. Natl. Acad. Sci. U.S.A.* **2006**, *103*, 12724−12728.
(38) Carl, P.; Kwok, C. H.; Manderson, G.; Speicher, D. W.; Discher, D. E. *Proc. Natl. Acad. Sci. U.S.A.* **2001**, *98*, 1565−1570.
(39) Ainavarapu, S. R.; Brujic, J.; Huang, H. H.; Wiita, A. P.; Lu, H.; Li, L.; Walther, K. A.; Carrion-Vazquez, M.; Li, H.; Fernandez, J. M. *Biophys. J.* **2007**, *92*, 225−233.
(40) Engstler, M.; Pfohl, T.; Herminghaus, S.; Boshart, M.; Wiegertjes, G.; Heddergott, N.; Overath, P. *Cell* **2007**, *131*, 505−515.
(41) Rispens, T.; Heer, P. O.-D.; Vermeulen, E.; Schuurman, J.; van der Neut Kolfschoten, M.; Aalberse, R. C. *J. Immunol.* **2009**, *182*, 4275−4281.
(42) Xiang, T.; Chumsae, C.; Liu, H. *Anal. Chem.* **2009**, *81*, 8101−8108.